Remote Sens. **2014**, *6*, 2008-2023; doi:10.3390/rs6032008

OPEN ACCESS

remote sensing

ISSN 2072-4292

www.mdpi.com/journal/remotesensing

Article

Identification of Soil Freezing and Thawing States Using SAR Polarimetry at C-Band

Thomas Jagdhuber [1,*], Julia Stockamp [1], Irena Hajnsek [1,2] and Ralf Ludwig [3]

[1] Microwaves and Radar Institute, German Aerospace Center, Münchener Strasse 20, D-82234 Wessling, Germany; E-Mail: julia.stockamp@dlr.de

[2] ETH Zürich, Schafmattstr. 6, CH-8093 Zurich, Switzerland; E-Mail: irena.hajnsek@ifu.baug.ethz.ch

[3] LMU Munich, Luisenstr. 37, D-80333 Munich, Germany; E-Mail: r.ludwig@lmu.de

***** Author to whom correspondence should be addressed; E-Mail: thomas.jagdhuber@dlr.de; Tel.: +49-8153-2329; Fax: +49-8153-1449.

Received: 29 November 2013; in revised form: 21 February 2014 / Accepted: 24 February 2014 / Published: 5 March 2014

Abstract: The monitoring of soil freezing and thawing states over large areas is very challenging on ground. In order to investigate the potential and the limitations of space-borne SAR polarimetry at C-band for soil state survey, analyses were conducted on an entire winter time series of fully polarimetric RADARSAT-2 data from 2011/2012 to identify freezing as well as thawing states within the soil. The polarimetric data were acquired over the Sodankylä test site in Finland together with *in situ* measurements of the soil and the snow cover. The analyses indicate clearly that the dynamics of the polarimetric entropy and mean scattering alpha angle are directly correlated to soil freezing and thawing states, even under distinct dry snow cover. First modeling attempts using the Extended Bragg soil scattering model justify the observed trends, which indicate surface-like scattering during frozen soil conditions and multiple/volume scattering for thawed soils. Hence, these first investigations at C-band foster motivation to work towards a robust polarimetric detection of soil freezing and thawing states as well as their transition phase.

Keywords: soil freezing; soil thawing; SAR polarimetry; polarimetric eigen-based decomposition; RADARSAT-2; C-band

---

1. Introduction

Monitoring of soil freezing and thawing states on large scales with high spatial and temporal resolution is especially important in high latitude ecosystems, as they affect the length of the growth season, the net primary production of organic matter, the carbon balance as well as frost damage on plants [1–5]. This requires an effective monitoring system, which is able to map the phase transitions within the soil and to monitor the extent as well as the temporal dynamics of the active layer in permafrost regions [6].

Investigations on soil states and its transitions started with the availability of ERS-1 C-band images in the early Nineties [7,8] and continued with the ENVISAT-mission [9], where the temporal behavior of single-polarization backscattering intensities were analyzed with respect to soil state changes [10]. Rignot *et al.* discovered a 3dB decrease in early winter, when the soil and vegetation freezes [5,8]. Wegmueller *et al.* report that frozen bare soil can be treated like dry soils due to the minimum in liquid water content [7]. However, Park *et al.* state that only distinct thaw and freeze-up periods could be monitored by intensity analysis. In addition, scatterometer data in two frequencies (Ku- and C-band) have been used to implement a probabilistic approach for freeze/thaw state determination of the soil with accuracies exceeding 90% for Siberian tundra (excluding rocky regions and areas with high soil moisture dynamics) [11]. In addition, Naemi *et al.* developed a Surface State Flag (SSF) from single-polarization ASCAT scatterometer data using an empirical threshold approach together with soil temperature data from the ECMWF reanalysis model as auxiliary information [12].

The availability of (fully) polarimetric information increases the ability to interpret and analyze different soil states and relates to the physical properties of the scatterers on ground (e.g., dielectric content of the soil) [13]. Concerning SAR polarimetry, first experimental studies have been undertaken to understand polarimetric SAR scattering signatures of (snow covered) soils for mapping freeze/thaw states of the soil [14,15]. Khaldoune *et al.* could allocate volume-type scattering mechanisms to thawed soil conditions, while surface-like scattering could be assigned to frozen soil conditions using airborne C-band data over the Bras d'Henri watershed, Canada [15]. Additional investigations proposed dual frequency, fully polarimeric SAR data, using PALSAR L-band [16] and RADARSAT-2 C-band [17] data, to investigate frozen and thawed soil conditions. In [17] a preliminary analysis of the canonical Freeman-Durden decomposition indicates dominant surface scattering over frozen soils for three agricultural test sites (Saskatchewan, Ontario, Quebec) in Canada. However, detailed scattering analyses of fully polarimetric data are still missing in order to assess the potential of polarimetric measurements for soil state monitoring.

In the following, a unique time series of RADARSAT-2 acquisitions along an entire winter period (2011/2012), supplemented by manifold *in situ* measurements, are investigated to evaluate the potential of SAR polarimetry at C-band (5.4 GHz) to identify soil freezing and thawing states. The test site and the experimental data from *in situ* measurements and SAR acquisitions of RADARSAT-2 are introduced in Section 2. The methodology for identification of soil freezing and thawing states is described in detail in Section 3 together with investigations on the behavior of the dielectric constant under freezing conditions. Results for soil state monitoring at C-band with fully polarimetric RADARSAT-2 data are shown in Section 4 followed by a summary in Section 5 and conclusions in Section 6.

2. Test Site and Experimental Data

A test site near the city of Sodankylä, northern Finland, at the location of the Finnish Meteorological Institute-ARC was selected, as indicated in Figure 1 [18,19]. The site is located 120 km north of the Arctic Circle and lies in the boreal/subarctic zone, exposed to continental climate. Two main land cover types are present for analysis of snow covered ground: Boreal forest and peatland/bog.

Figure 1. Test site location (red box) near the city of Sodankylä, Finland, and C-band RGB image of a Pauli decomposition showing the surroundings of the test site (R: Double bounce scattering, G: Volume scattering, B: Surface soil scattering) as well as a zoom into a modified aerial image of the local measurement locations (green circles) around the FMI-ARC within the test site (AWS, IOA, RefIOA, Forest, Peatland, Bog1, Bog2, Bog2G, Bog3); SWE = Snow Water Equivalent [18].

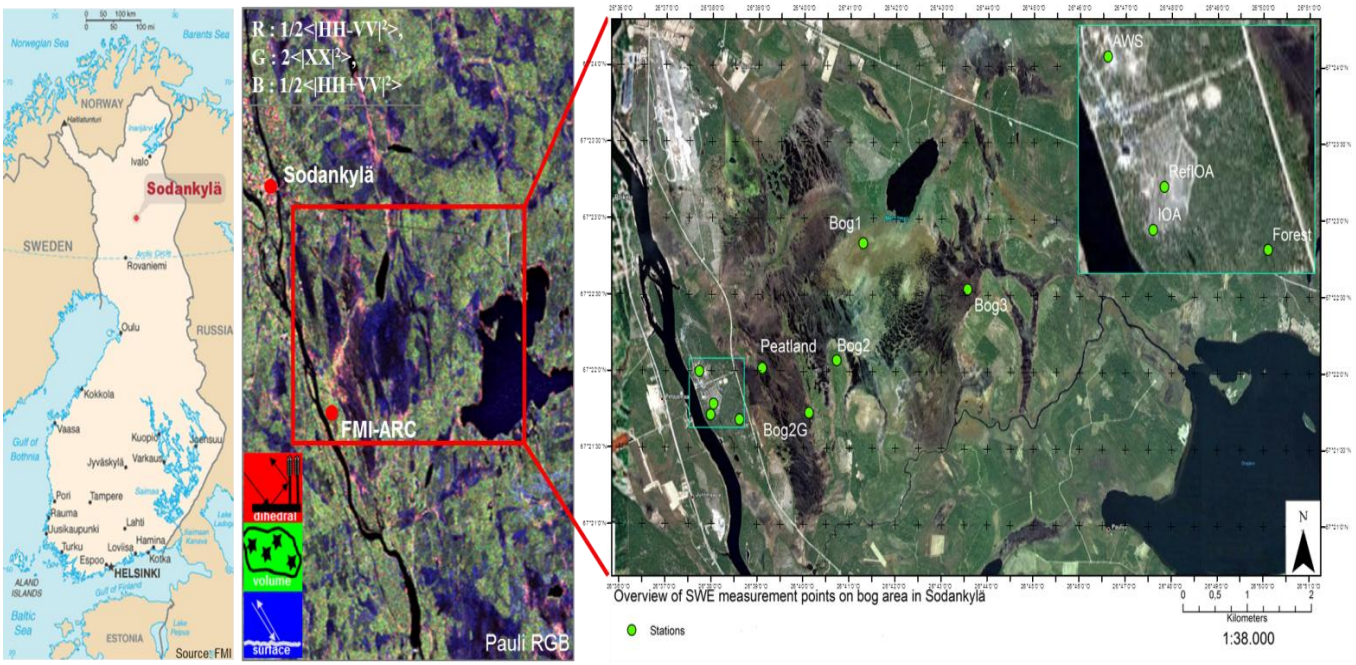

Figure 1 shows the seven ground locations for reference measurements (green circles within the figure: AWS, IOA, RefIOA, Forest, Peatland, Bog1, Bog2, Bog2G, Bog3). For the locations AWS (Automatic Weather Station) and IOA (Intensive Observation Area), automatic recording stations enabled the acquisition of several geo-physical parameters, as for example snow density, soil temperature, air temperature, wind and snow fall [18,19]. Figure 2 shows, exemplarily for the IOA, the temporal evolution of the snow parameters within the entire winter period 2011/2012 (beginning of November 2011 until middle of June 2012) together with the acquired fine quad-polarimetric RADARSAT-2 data indicated as blue, vertical lines. A distinct snow cover of maximum 100 cm depth developed in the respective winter. The soil started to freeze in the middle of December 2011 (~15 December 2011, air and soil temperature < 0 °C) and thawed in the beginning of June 2012 (~18 May 2012, air and soil temperature > 0 °C) (see red and golden lines in Figure 2).

Figure 2. Snow depth (blue), air (red) and soil (orange) temperature curves recorded at the IOA measurement site (a forest clearing, where the ground vegetation consists of low lichen, moss and heather) for the entire winter period from snow accumulation starting in November 2011 until snow free periods in June 2012. The blue, vertical, dashed lines indicate the acquisition dates of RADARSAT-2: 8.11.11, 2.12.11, 26.12.11, 19.1.12, 12.2.12, 7.3.12, 31.3.12, 24.4.12, 18.5.12, 11.6.12 [19].

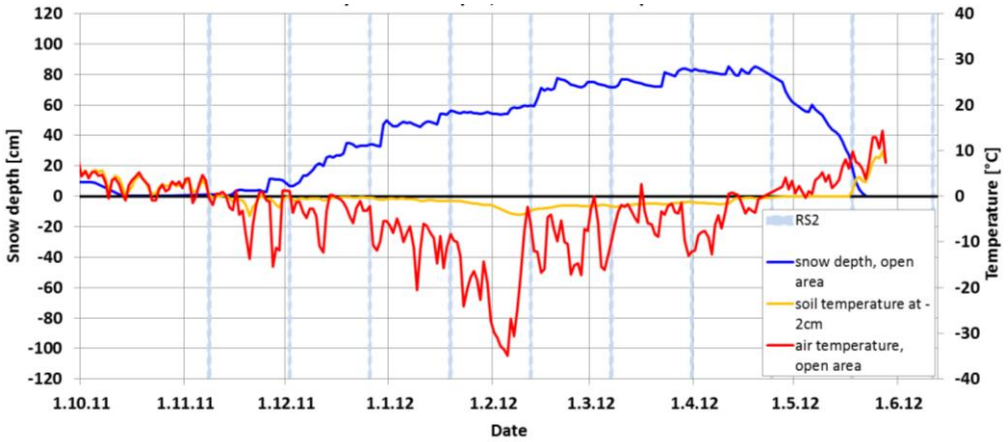

The air temperature reached down to −30 ℃ at some days in this winter. This indicates the development of a dry snow cover and a frozen upper soil, which can be characterized by *in situ* and SAR remote sensing techniques.

For the Sodankylä test site the RADARSAT-2 instrument acquired quad-polarimetric data with a spatial resolution of 5.2 m × 7.6 m (slant range × azimuth) starting from 8th of November 2011. With a repeat cycle of 24 days, a time series of ten fully polarimetric RADARSAT-2 C-band data at 33.2° incidence enabled an investigation of the complete winter period 2011/2012 from snow accumulation to snow melt. The RADARSAT-2 C-band data are complemented with *in situ* ground measurements of snow water equivalent (SWE), snow depth, soil moisture, soil and air temperature for analysis and validation [19].

3. Methodology of Identifying Soil Freezing and Thawing States

The identification of freezing and thawing soil states implies the knowledge of the change in soil moisture and dielectric constant, which can be tracked by polarimetric SAR [20]. For the change in soil dielectric constant, the phase transition from liquid to frozen water (and back) has to be modeled in order to understand its effect on the polarimetric observables.

3.1. Impact of Phase Transitions on the Dielectric Constant of Soils

For studying the impact of phase transitions on the dielectric constant of soils the well-known semi-empirical dielectric mixing model of Dobson was extended by Zhang *et al.* to include freezing conditions (T < 0 ℃) [21,22]. New terms m_{vi} and m_{vu} are introduced in [22] to account for the ice and unfrozen moisture contribution to the soil dielectric constant. For the range of 1.4 to 18 GHz,

the dielectric mixing model for the real ε'_{mf} and imaginary part ε''_{mf} of the relative complex dielectric constant ε_{mf} are derived from [21–23] including also negative soil temperatures:

$$\varepsilon'_{mf} = \left(1+\left(\frac{\rho_b}{\rho_s}\right)\left(\varepsilon_s^{\alpha}-1\right)+m_{vu}^{\beta'}\left(\varepsilon'_{fw}\right)^{\alpha}-m_{vu}+m_{vi}\varepsilon_i^{\alpha}\right)^{1/\alpha} \quad (1)$$

$$\varepsilon''_{mf} = m_{vu}^{\beta''/\alpha}\varepsilon''_{fw} \quad (2)$$

where ρ_b is the bulk density, ρ_s is the soil density, α and β are empirical coefficients defined in [21,22]. The dielectric constant of ice ε_i is set to 3.15. The dielectric constant of soil solids ε_s is set to 4.7 and ε_{fw} is the dielectric constant of free water. m_{vu} is the unfrozen volumetric moisture content and m_{vi} is the volumetric ice content. The real and imaginary parts of the dielectric constant of free water ε_{fw} in Equations (1) and (2) are defined in [23]. m_{vu} and m_{vi} are given by [22]:

$$m_{vu} = A\left|T-273.2\right|^{-B}\rho_b\rho_w \quad (3)$$

$$m_{vi} = \left(m_v - m_{vu}\right)\rho_w/\rho_i \quad (4)$$

with A and B being empirical soil texture parameters (see Table 1) and T is the absolute soil temperature in Kelvin steering the amount of liquid to frozen water in the soil. For the specific density of water ρ_w a value of 1.0 g/cm^3 and for the specific density of ice ρ_i a value of 0.9175 g/cm^3 are assumed.

Figure 3 displays modeled phase transitions for different soils from silty clay to sandy loam as well as for different frequencies from C- to Ku-band. As soon as the soil temperature falls below zero degree Celsius, a distinct drop of ε'_{mf} occurs for all soil types and all frequencies, which keeps the dielectric level close to the lower physical limit for all freezing states. Hence, this sharp decrease is expected to have an effect on the polarimetric observables to distinguish freezing and thawing states of the soil.

Figure 3. Modeling of soil phase transition (freezing-thawing) with the Dobson/Zhang-dielectric mixing model as function of soil temperature steering the amount of liquid to frozen water in the soil; (**a**): ε'_{mf} for different soil types at C-band (5 GHz); (**b**): ε'_{mf} of different frequencies from C- (5 GHz), X- (10.6 GHz) to Ku- (23.8 GHz) band for soil of sandy loam.

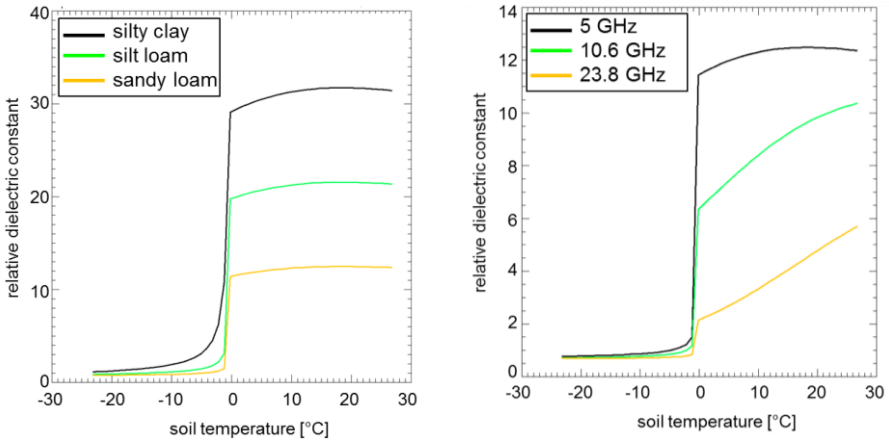

(**a**) (**b**)

Table 1. Empirically derived soil texture parameters for the dielectric mixing model of [22].

Soil Type	Sand (%)	Silt (%)	Clay (%)	ρ_b	ρ_s	A	B
Silty clay	6.83	45.76	47.41	1.62	2.60	11.3301	0.6166
Silt loam	28.58	51.46	19.96	1.58	2.58	5.2752	0.5675
Sandy loam	50.73	39.61	9.66	1.59	2.63	2.6945	0.6104

3.2. Polarimetric Eigen-Based Decomposition

In order to investigate and reveal the freezing or thawing state of the soil a polarimetric eigen-based decomposition of the fully polarimetric SAR data is performed. Therefore the coherency matrix [*T*] of the fully polarimetric RADARSAT-2 data is formed with an averaging of 9 × 9 pixels resulting in 81 looks and is decomposed afterwards as follows [24,25]:

$$\langle [T] \rangle = \lambda_1 \cdot e_1 \cdot e_1^{T^*} + \lambda_2 \cdot e_2 \cdot e_2^{T^*} + \lambda_3 \cdot e_3 \cdot e_3^{T^*} \tag{5}$$

where λ_i are the positive, real-valued eigenvalues and e_i the corresponding, complex-valued, normalized eigenvectors. T^* denotes the transpose conjugate.

The mean polarimetric scattering alpha angle α is derived from the normalized eigenvectors of Equation (5), indicating an intrinsic scattering type ranging from surface scattering ($\alpha = 0$) to volume scattering ($\alpha = \pi/4$) until dihedral scattering ($\alpha = \pi/2$) and is calculated as follows [24,25]:

$$\alpha = \sum_{i=1}^{n} P_i \cdot \operatorname{acos}\left(|e_{i1}|\right), \quad e_i = \begin{bmatrix} e_{i1} & e_{i2} & e_{i3} \end{bmatrix}^T \tag{6}$$

Therefore α relates directly to the dominant physical scattering mechanism of the scatterers in the resolution cell, which is visualized in Figure 4.

Figure 4. Physical meaning of the dominating intrinsic scattering mechanism expressed by the mean alpha scattering angle (ranging from surface scattering $\alpha = 0$ to dihedral scattering $\alpha = \pi/2$).

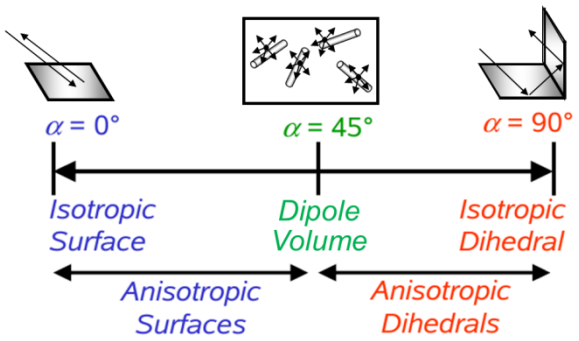

In order to evaluate the statistical disorder and thereby the diversity of scattering mechanisms occurring in the resolution cell, the scattering entropy H is investigated [24,25].

$$H = \sum_{i=1}^{n} -P_i \log_n P_i \qquad P_i = \lambda_i / \sum_{j=1}^{n} \lambda_j \tag{7}$$

where P_i is a pseudo-probability and n equals three (for the monostatic RADARSAT-2 system).

The entropy *H* indicates the depolarization of the acquired microwave signal. An entropy close to zero indicates one (almost deterministic) non-depolarizing scattering process, while an entropy near one represents fully depolarizing, random scattering with several scattering mechanisms involved.

During freezing of the soil, the dielectric constant of the soil decreases distinctively (see Figure 3). Hence, the polarimetric entropy and the mean scattering alpha angle should tend to lower values indicating a less complex, surface-like scattering due to the low dielectric contrast in all scattering components of the resolution cell.

In contrast, soil thawing will increase the dielectric contrast among the scattering component in the resolution cell, and increase the polarimetric entropy and the mean scattering alpha angle to more complex scattering scenarios of multiple scattering mechanisms. These behaviors will be modelled in a first attempt by the surface scattering model in Section 3.3.

In order to understand the different scattering mechanisms in more detail, Cloude and Pottier developed the following segmentation scheme of the so-called entropy-alpha plane for L-band (see Figure 5) [26,27], which is applied to C-band RADARSAT-2 data in Section 4. It is expected that surface scattering located in the lower left corner for L-band in Figure 5 will shift to higher entropy values located in the 'random surface' segment for C-band.

Figure 5. Scattering plane of polarimetric entropy and mean scattering alpha angle with the segmentation scheme of Cloude and Pottier indicating different scattering types (originally developed for L-band) [26,27].

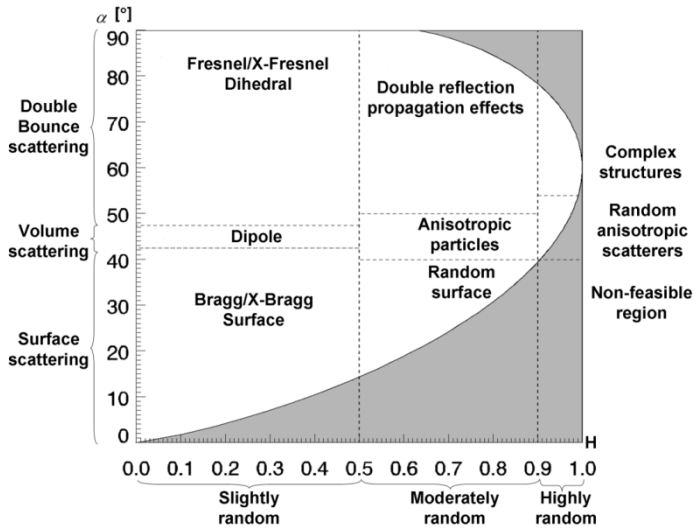

3.3. Modeling of Soil Surface Scattering from Frozen and Thawed Soils

In order to simulate the surface scattering from freezing and thawing soils, the distinct drop/rise in dielectric constant, when the soil freezes/thaws is included in a first modeling attempt with the extended Bragg (X-Bragg) model. This surface scattering model for bare soils was developed in [28] and accounts for changes in soil moisture/dielectric constant ε'_{mf} and in soil roughness by a depolarization angle δ [20]:

$$[T_{XB}] = f_s \begin{bmatrix} 1 & \beta^* \sin c(2\delta) & 0 \\ \beta \sin c(2\delta) & \frac{1}{2}|\beta|^2 (1+\sin c(4\delta)) & 0 \\ 0 & 0 & \frac{1}{2}|\beta|^2 (1-\sin c(4\delta)) \end{bmatrix} \quad (8)$$

This scattering model $[T_{XB}]$ for rough surfaces consists of a surface scattering intensity f_S and a surface scattering mechanism β. Both components are modeled by means of the *Bragg* scattering coefficients (R_H, R_V), which are function of ε'_{mf} and the local incidence angle θ [20]:

$$f_S = \frac{m_S^2}{2}|R_H + R_V|^2 \quad , \quad \beta = \frac{R_H - R_V}{R_H + R_V} \quad (9)$$

Hence, this surface scattering model can be driven in a forward sense for a range of reasonable soil moisture (as function of ε'_{mf} from 2 to 41) and soil roughness values (as function of δ from 0 ° to 90 °). Afterwards, the polarimetric eigen-based decomposition can be applied to the modelled $[T_{XB}]$ and the resulting polarimetric entropy and mean scattering alpha angles of the surface scattering can be analyzed and compared with the data-derived counterparts of the two polarimetric parameters. It is important to note that the modelled surface scattering does not include any contribution from a possible vegetation cover.

4. Results for Identification of Different Soil States

On each of the ten fine quad-polarimetric RADARSAT-2 scenes the polarimetric, eigen-based decomposition was applied for the entire winter period from beginning of November 2011 until middle of June 2012. The scattering entropy H and mean scattering alpha angle α have been calculated and are shown in Figure 6. The red bars indicate the transition periods for the soil towards freezing in the beginning of the winter (end of November/beginning of December 2011) and towards thawing in the end of the winter (April 2012).

Concurrently, a decreasing trend of the eigen-based decomposition parameters during soil phase transition towards freezing ($H \rightarrow 0.4$–0.7, $\alpha \rightarrow 15$ °–30 °) and an increasing trend for transition towards thawing ($H \rightarrow 0.7$–1.0, $\alpha \rightarrow 30$ °–50 °) is apparent. The white circle in Figure 6 indicates the Sodankyl ätest site with similar dynamics.

In order to investigate the sensitivity of C-band to state transitions of the soil on the local scale, Figure 7 reveals the trends of the respective eigen-based parameters for all investigated measurement locations within the test site taking an area of 11 × 11 pixels around each measurement location for analysis. Also the soil moisture measurements at 2 cm depth from two continuously recording moisture sensors of the IOA (at location A and B) are displayed as *in situ* reference. Congruent dynamics and trends, compared to Figure 6, are recognizable for the single locations including areas of different land use (bog, peat, boreal forest). Hence, the comparison of the eigen-based parameters with soil moisture *in situ* measurements in Figure 8 and with the soil and air temperature in Figure 2 state the connection to the soil freezing and thawing states rather clearly. However, the spatial variation of the polarimetric entropy and mean scattering alpha values at a given date (under either frozen or unfrozen conditions) also exhibit a distinct variation, which can be attributed to the spatially heterogeneous land cover and

most probably also to soil types. Unfortunately, only land use information and no detailed soil map or soil profiles are available for the test site area.

Figure 6. Polarimetric scattering entropy and mean scattering alpha angle for the RADARSAT-2 time series at C-band covering the entire winter period 2011/2012; White circle indicates the Sodankyl ätest site; The red bars indicate the beginning and the end of the soil frost period with always one scene in the phase transition period of the soil [18].

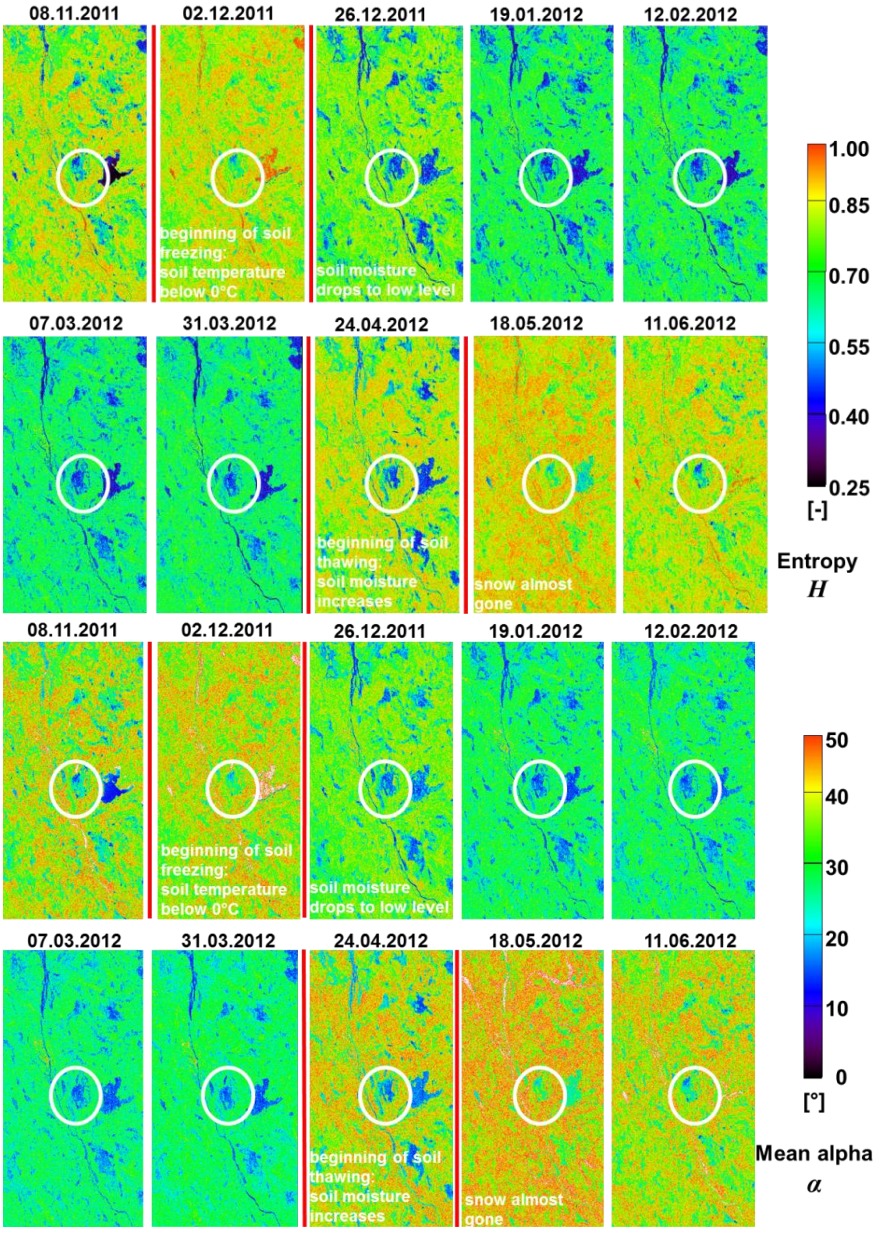

Figure 7. Analysis of polarimetric entropy and mean scattering alpha angle for different measurement locations (colors of curves) compared with soil moisture measurements at 2 cm depth from two continuously recording moisture sensors at location A and B within the IOA (bottom plot); Red vertical bars indicate the soil frost period.

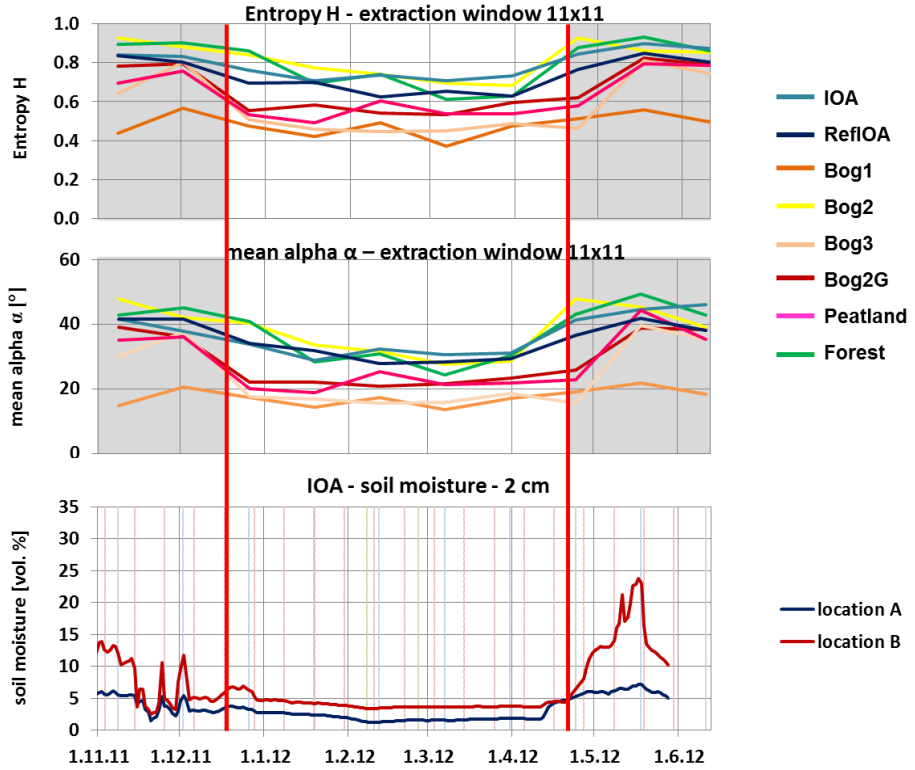

Figure 8. 2D-Histograms of polarimetric entropy *vs.* mean scattering alpha angle from the peatland measurement site (see Figure 1 for localization) covering the entire winter period 2011/2012; Red bars indicate the phase transitions of the soil; The color inside the plots indicate the number of counts from low (gray-blue) to high (orange-red).

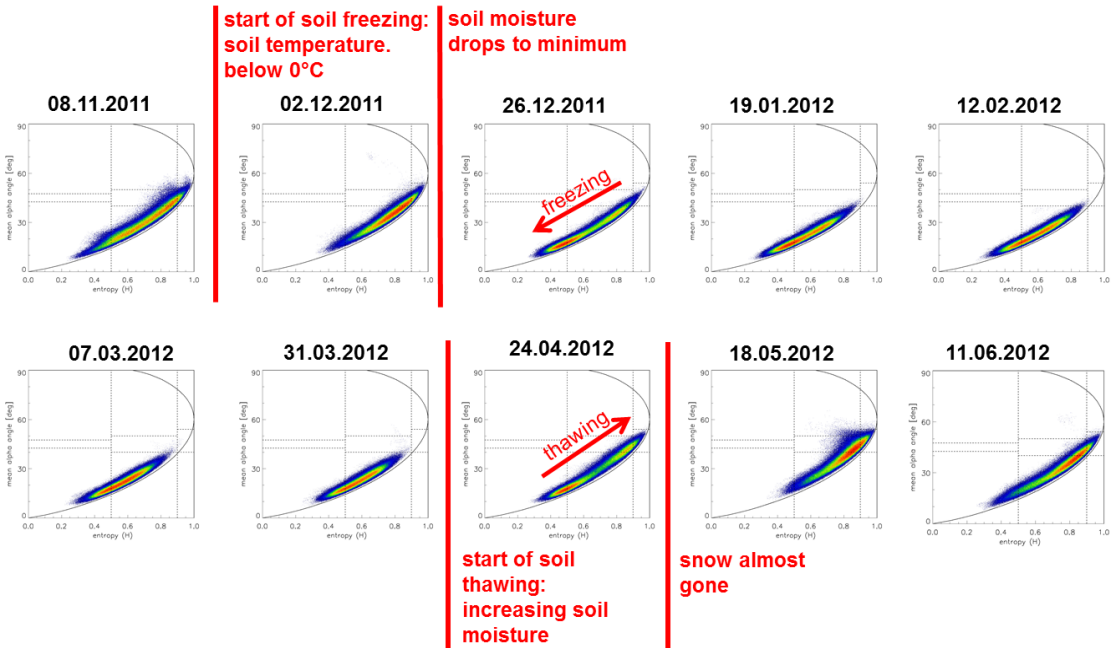

Focusing further on the peatland measurement site assuring no forest or distinct vegetation disturbance Figure 8 presents two dimensional (2D)-histograms of the polarimetric entropy and the mean scattering alpha angle for the entire time span covering the winter period 2011/2012 (see Figure 5 for introduction of physical meaning of the 2D-histogram). The majority of *H*-*α* value couples indicated by the red zone (high counts within the 2D-histogram) confirm the observed dynamics again. The polarimetric entropy and mean scattering alpha values decrease significantly with the occurrence of soil freezing and rise again as soon as thawing conditions occur in the end of the winter in Sodankylä.

Moreover the absolute difference of polarimetric entropy (delta entropy) and of mean scattering alpha (delta mean alpha angle) values of the entire RADARSAT-2 scene and the peatland measurement site (see Figure 1 for measurement point) are depicted as three combinations of frozen and unfrozen soil states in Figure 9:

1. Δ*H*/Δ*α*-Case: Comparison of frozen state (19.1.2012) with frozen state (12.2.2012); Absolute differences are small and mainly centered around zero.
2. Δ*H*/Δ*α*-Case: Comparison of frozen state (12.2.2012) with unfrozen state (18.5.2012); Absolute differences are large and centered around 0.2/15 ° for ΔH/Δα.
3. Δ*H*/Δ*α*-Case: Comparison of unfrozen state (18.5.2012) with unfrozen state (11.6.2012); Absolute differences are small and mainly centered around zero.

Figure 9. Comparison between the absolute difference of polarimetric entropy (delta entropy) and of mean scattering alpha (delta mean alpha angle) values of the entire RADARSAT-2 scene (**a,b,c**) and the peatland measurement site (**d,e,f**) for two soil states; (a,d): Frozen state (19.1.)–frozen state (12.2.); (b,e): Frozen state (12.2.)–unfrozen state (18.5.); (c,f): Unfrozen state (18.5.)–Unfrozen state (11.6.); The color inside the plots indicate the number of counts from low (gray-blue) to high (orange-red).

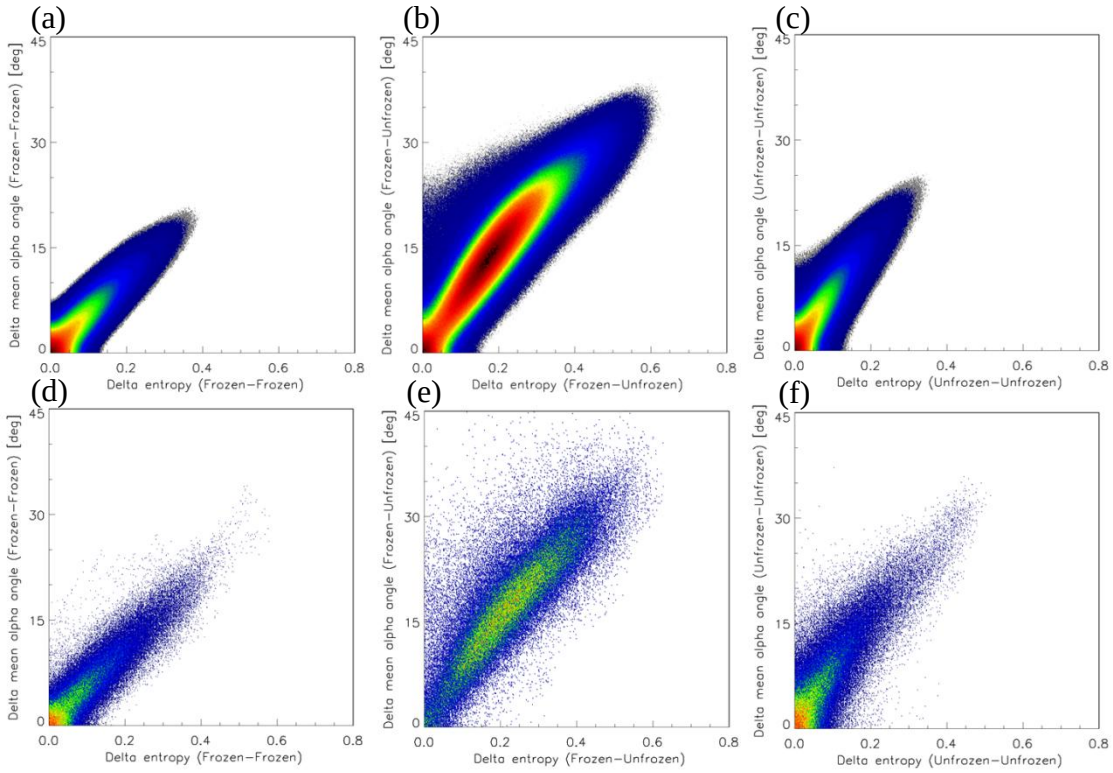

In addition, the analysis with the scattering mechanism classification for these *H*-α planes (dashed lines in Figures 8 and 10), proposed in [26] for L-band and shown in Figure 5, suggests a transition from volume-like scattering to surface-like scattering, when the soil freezes, and back under thawing conditions in April 2012. This confirms the model predictions in the methodology section. But as we are dealing with C-band data, this classification (developed originally for L-band wavelength) should give a first indication of possible physical scattering mechanisms and is still under investigation.

Figure 10. Comparison between data-derived RADARSAT-2 at the peatland measurement site and model-derived X-Bragg polarimetric entropy and mean scattering alpha values; The color in the data plots indicate the number of counts from low (gray-blue) to high (orange-red); Red arrows indicate major dynamics of data and modeled values (only soil scattering).

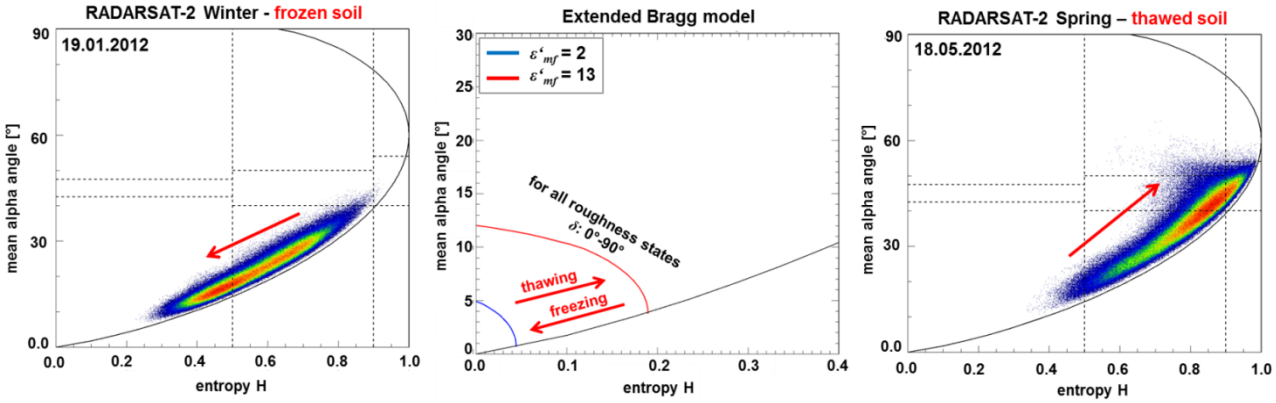

In order to turn to a more quantitative analysis the Extended Bragg scattering model of Equation (8) was taken and fed with two different real parts of the dielectric constant simulating freezing ($\varepsilon'_{mf} = 2$) and thawing ($\varepsilon'_{mf} = 13$) upper soil conditions according to the Dobson/Zhang model output in Figure 3. In addition the soil roughness, represented by the depolarization angle δ, was varied over the whole range of physically possible roughness states from smooth ($\delta = 0°$) until very rough ($\delta = 90°$). Afterwards the polarimetric entropy and mean scattering alpha angle values were calculated for all simulated states.

Figure 10 reports the results of the X-Bragg-modeled and the SAR-derived dynamics of polarimetric entropy and mean scattering alpha angles. Hence, the trend of the shift for both eigen-based parameters (H, α) is the same and links the changes in soil state with the behavior of the respective polarimetric parameters. However, a direct inversion of the dielectric content of frozen/unfrozen soils cannot be established for the RADARSAT-2 C-band data, as the applied surface scattering model was initially developed for longer wavelengths and only reproduces the general trends. In addition, the scattering scenario is here modeled in a first attempt neglecting any contributions from the vegetation cover, which is most likely causing the higher entropy-regime in the SAR data-derived values. Hence, a further step will be the inclusion of a bog-like vegetation disturbance in the modeling of the scattering scenario in order to better represent the observed scattering mechanisms. This could be realized by a polarimetric particle scattering model representing the main plant constituents of the bog vegetation cover as introduced in [25] and investigated in detail for agricultural vegetation in [27].

5. Summary

A time series consisting of ten fine quad-polarimetric RADARSAT-2 scenes over the Sodankylä test site in Northern Finland were analyzed for sensitivity to soil freezing and thawing states using SAR polarimetry. The comparison of *in situ* measurements of the FMI-ARC for soil moisture as well as soil temperature with the polarimetric entropy and mean scattering alpha angle from an eigen-based decomposition revealed a strong relation between the drop ($H \rightarrow 0.4–0.7$, $\alpha \rightarrow 15°–30$) of the polarimetric parameters with soil freezing (frozen state) and the rise ($H \rightarrow 0.7–1.0$, $\alpha \rightarrow 30°–50°$) of the latter, when the soil thaws again (unfrozen state). Modeling of the observed eigen-based dynamics with the polarimetric surface scattering model X-Bragg and the dielectric mixing model of Dobson/Zhang for the change in soil dielectric constant resulted in similar trends compared to the shift observed for the SAR-based counter parts. However, these first modeling attempts just consider a basic scattering scenario and need to be extended to a more sophisticated case in future investigations.

6. Conclusions

The presented results in Section 4 state that C-band exhibits sensitivity to soil freezing/thawing states, even under distinct dry snow cover (up to 100 cm), which can be traced by a fully polarimetric, time series analysis using an eigen-based decomposition technique. The different soil states can be clearly detected and also the transition phase can be identified to a first extend (in terms of weeks), as the soil freezing and thawing states directly affect the dynamics of the polarimetric entropy and mean scattering alpha angle.

However, for a precise detection of the beginning and the end of the transition phase (in terms of days), longer time series including several freezing thawing cycles are needed to obtain a broader basis set for a robust statistical analysis of appropriate thresholds. This indicates the need of a short SAR temporal coverage to conveniently identify the start and the length of the transition phase. Fortunately, this will be met by the installation of the RADARSAT constellation to further improve the temporal coverage.

In addition, first modeling attempts using the Extended Bragg soil scattering model justify the observed trends, which indicate surface-like scattering during frozen soil conditions and multiple/volume scattering for thawed soils. However, a direct inversion of the dielectric constant from frozen/thawed soil is not yet possible, as adaptions/extensions of the soil scattering model are necessary. If this can be established, it should be possible to polarimetrically decompose different scattering components coming from the soil and the vegetation as well as directly track the soil dielectric constant for phase transitions and soil states. Hence, these first investigations at C-band foster motivation to work towards a robust polarimetric detection of soil freezing and thawing states as well as their transition phase.

Acknowledgments

The authors gratefully acknowledge Konstantinos P. Papathanassiou for numerous helpful suggestions as well as proof-reading of the manuscript, Juha Lemmetyinen as well as colleagues from the Arctic Research Centre of Finish Meteorological Institute (FMI-ARC) for *in situ* data supply and Silvan Leinss from ETH Zurich for helpful support with *in situ* data processing. MacDonald, Dettwiler and Associates

Ltd. (MDA), the Canadian Space Agency (CSA), the Canada Centre for Remote Sensing (CCRS) and the European Space Agency (ESA) are gratefully acknowledged for supporting the activities. The research work was conducted under the ESA-funded project ALGOSNOW (ESA-contract number: 4000103180/11/NL/CT). Radarsat-2 C-band data were provided via the Science and Operational Applications Research for RADARSAT-2 (SOAR) program proposal (nr. 5071). In addition, the authors want to thank the anonymous reviewers for their valuable comments and helpful suggestions.

Author Contributions

Thomas Jagdhuber and Julia Stockamp carried out the data analyses and wrote the manuscript. Irena Hajnsek and Ralf Ludwig supervised the research efforts. All authors compiled and approved the final manuscript.

Conflicts of Interest

The authors declare no conflict of interest.

References

1. Khovorostynaov, D.V.; Ciais, P.; Krinner, G.; Zimov, S.A.; Corradi, Ch.; Guggenberger, G. Vulnerability of permafrost carbon to global warming. Part II: Sensitivity of permafrost carbon stock to global warming. *Tellus* **2008**, *60*, 265–275.
2. Goulden, M.L.; Wofsky, S.C.; Harden, J.W.; Trumbore, S.E.; Crill, P.M.; Gower, S.T.; Fries, T.; Daube, B.C.; Fan, S.-M.; Sutton, D.J.; *et al.* Sensitivity of boreal forest carbon balance to soil thaw. *Science* **1998**, *279*, 214–217.
3. Torre Jorgenson, M.; Romanovsky, V.; Harden, J.; Shur, Y.; O'Donnell, J.; Schuur, E.A.G.; Kanevskiy, M.; Marchenko, S. Resilience and vulnerability of permafrost to climate change. *Cand. J. For. Res.* **2010**, *40*, 1219–1236.
4. Rignot E.; Way, J.B. Monitoring freeze-thaw cycles along North-South Alaskan transects using ERS-1 SAR. *Remote Sens. Environ.* **1994**, *49*, 131–137.
5. Smith, N.V.; Saatchi, S.S.; Randerson, J.T. Trends in high northern latitude soil freeze and thaw cycles from 1988 to 2002. *J. Geophys. Res.* **2004**, *109*, 1–14.
6. Schuur, E.A.G.; Bockheim, J.; Canadell, J.G.; Euskirchen, E.; Field, C.B.; Goryachkin, S.V.; Hagemann, S.; Kuhry, P.; Lafleur, P.M.; Lee, H.; *et al.* Vulnerability of permafrost carbon to climate change: Implications for the global carbon cycle. *BioScience* **2008**, *58*, 701–771.
7. Wegmüller, U. The effect of freezing and thawing on the microwave signatures of bare soil. *Remote Sens. Environ.* **1990**, *33*, 123–135.
8. Rignot, E.; Way, J.B.; McDonald, K.; Viereck, L.; Williams, C.; Adams, P.; Payne, C.; Wood, W.; Shi, J. Monitoring of environmental conditions in taiga forests using ERS-1 SAR. *Remote Sens. Environ.* **1994**, *49*, 145–154.
9. Park, S.-E.; Bartsch, A.; Sabel, D.; Wagner, W.; Naeimi, V.; Yamaguchi, Y. Monitoring freeze/thaw cycles using ENVISAT ASAR global mode. *Remote Sens. Environ.* **2011**, *115*, 3457–3467.

10. Li, Z.; Guo, H. Permafrost Mapping in the Tibet Plateau Using Polarimetric SAR. In Proceedings of the 2000 IEEE International Symposium on Geoscience and Remote Sensing, Honolulu, HI, USA, 24–28 July 2000; pp. 2024–2026.
11. Zwieback, S.; Bartsch, A.; Melzer, T.; Wagner, W. Probabilistic fusion of Ku and C-band scatterometer data for determining the freeze/thaw state. *IEEE Trans. Geosci. Remote Sens.* **2012**, *50*, 2583–2594.
12. Naeimi, V.; Paulik, C.; Bartsch, A.; Wagner, W.; Kidd, R.; Park, S.-E.; Elger, K.; Boike, J. ASCAT Surface State Flag (SSF): Extracting information on surface freeze/thaw conditions from backscatter data using an empirical threshold-analysis algorithm. *IEEE Trans. Geosci. Remote Sens.* **2012**, *7*, 2566–2582.
13. Mironov, V.L.; Komarov, S.A.; Li, S.; Romanovsky, V.E. Freeze-Thaw Processes Radar Remote Sensing: Modeling and Image Processing. In Proceedings of the 2005 IEEE International Symposium on Geoscience and Remote Sensing, Seoul, South Korea, 25–29 July 2005; pp. 608–611.
14. Lee, J.-S.; Pottier, E. *Polarimetric Radar Imaging: From Basics to Applications*; Taylor & Francis: Boca Raton, FL, USA, 2009.
15. Khaldoune, J.; van Bochove, E.; Bernier, M.; Nolin, M.C. An Approach for Mapping Frozen Soil of Agricultural Land under Snow Cover Using RADARSAT-1 and RADARSAT-2. In Proceedings of 2008 IEEE International Symposium on Geoscience and Remote Sensing, Boston, MA, USA, 8–11 July 2008; pp. 382–385.
16. Longepe, N.; Tadono, T.; Shimada, M.; Pottier, E.; Allain, S. Case Studies of Frozen Ground Monitoring Using PALSAR/ALOS Data. In Proceedings of the 2009 IEEE International Symposium on Geoscience and Remote Sensing, Cape Town, South Africa, 12–17 July 2009; pp. 1020–1023.
17. Rousseau, L.-P.; Magagi, R.; Leconte, R.; Berg, A.; Toth, B. Potentials of RADARSAT-2 Data to Monitor Freezing/Thawing Cycles over Agricultural Lands in Canada. In Proceedings of the International Symposium on Geoscience and Remote Sensing, Cape Town, South Africa, 12–17 July 2009; pp. 598–601.
18. Stockamp, J.; Jagdhuber, T.; Parrella, G.; Hajnsek, I.; Ludwig, R. Multi-Frequency Analysis of Snow-Covered Areas Using SAR Polarimetry. In Proceedings of the 6th International Workshop on Science and Applications of SAR Polarimetry and Polarimetric Interferometry, ESA-ESRIN, Frascati, Italy, 28 January–1 February 2013.
19. Finnish Meteorological Institute (FMI) Database of Arctic Research Centre. Available online: http://litdb.fmi.fi/ (accessed on 20 March 2013).
20. Hajnsek, I.; Jagdhuber, T.; Schoen, H.; Papathanassiou, K.P. Potential of estimating soil moisture under vegetation cover by means of PolSAR. *IEEE Trans. Geosci. Remote Sens.* **2009**, *47*, 442–454.
21. Dobson, M.C.; Ulaby, F.T.; Hallikainen, M.T.; El-Rayes, M.A. Microwave dielectric behavior of wet soil—Part II: Dielectric mixing models. *IEEE Trans. Geosci. Remote Sens.* **1985**, *GE-23*, 35–46.

22. Zhang, L.; Shi, J.; Zhang, Z.; Zhao, K. The Estimation of Dielectric Constant of Frozen Soil-Water Mixture at Microwave Bands. In Proceedings of 2003 IEEE the International Symposium on Geoscience and Remote Sensing, Toulouse, France, 21–25 July 2003; pp. 608–611.
23. Peplinski, N.R.; Ulaby, F.T.; Dobson, M.C. Dielectric properties of soils in the 0.3–1.3-GHz range. *IEEE Trans*. *Geosci*. *Remote Sens*. **1995**, *33*, 803–807.
24. Cloude, S.R.; Pottier, E. A review of target decomposition theorems in radar polarimetry. *IEEE Trans*. *Geosci*. *Remote Sens*. **1996**, *34*, 498–518.
25. Cloude, S.R. *Polarisation: Applications in Remote Sensing*; Oxford University Press: Oxford, UK, 2010.
26. Cloude, S.R.; Pottier, E. An entropy based classification scheme for land applications of polarimetric SAR. *IEEE Trans*. *Geosci*. *Remote Sens*. **1997**, *35*, 68–78.
27. Jagdhuber, T. Soil Parameter Retrieval under Vegetation Cover Using SAR Polarimetry. Ph.D. Thesis, University of Potsdam, Potsdam, Germany, 2012.
28. Hajnsek, I.; Pottier, E.; Cloude, S.R. Inversion of surface parameters from polarimetric SAR. *IEEE Trans*. *Geosci*. *Remote Sens*. **2003**, *41*, 727–744.